

# Backward Scattering of Electrically Large Standard Objects Illuminated by OAM Beams

Kang Liu<sup>ID</sup>, Hongyan Liu<sup>ID</sup>, Wei E. I. Sha<sup>ID</sup>, Yongqiang Cheng<sup>ID</sup>, and Hongqiang Wang

**Abstract**—To evaluate the interaction between the orbital angular momentum (OAM) beams and the electrically large standard objects, the backward scattering characteristics of the perfect electrical conductor (PEC) sphere and PEC cone are studied. First, the incident vortex electromagnetic field carrying OAM is generated by Hertzian dipole arrays. Subsequently, the backward-scattered field is calculated by the physical optics algorithm. The phase profiles and OAM spectra are analyzed in detail, which indicates that the scattered field for axial symmetric objects still keeps the main characters of the vortex field due to the angular momentum conservation. Finally, the radar cross section for PEC sphere and cone are calculated, respectively. The backward scattering features show significant differences when OAM beams change their topological charges. Consequently, given a specific propagation direction, compared to plane waves, more information will be offered by the OAM beams for object detection and recognition.

**Index Terms**—Orbital angular momentum (OAM), physical optics (PO), radar cross section (RCS), vortex electromagnetic wave.

## I. INTRODUCTION

OVER the past few years, electromagnetic waves carrying orbital angular momentum (OAM) have been applied in wireless communications [1], rotational Doppler detection [2], and radar imaging [3]. Many approaches about the multiplexing and demultiplexing of OAM beams, OAM measurement, and OAM target imaging are proposed. However, the interaction between OAM beams and the electrically large object is still a challenging problem to be solved, especially for OAM's applications in radar realms [4].

To the best of our knowledge, only a few publications have studied the scattering characteristics of OAM beams. Compared with plane waves, the OAM beams have helical wavefronts with different topological charges, which is expected to lead to different and rich scattering phenomena when illuminating the object. In [5], the scattering from a zero-order Bessel beam by a dielectric sphere was reported. In [6], the finite-difference

time-domain technique is applied to calculate the scattering from the Laguerre–Gaussian beams by dielectric particles. In [7], the scattering problem of chaff clouds was studied, and results show that the information carried by the OAM beams can pass through the chaff clouds easier than the plane waves. In 2018, the measured RCS values of corner reflectors and flat plate in an anechoic chamber were reported [8]. From the works of literature above, some distinct characters of the OAM scattering have been found. However, the high-frequency scattering characteristics of electrically large objects illuminated by OAM beams have not been studied yet. From high-frequency scattering theory, the backward scattering of electrically large objects dominantly depends on its strong scattering centers. But the argument based on plane wave incidence is not applicable to OAM beams, and the scattering center may disappear due to zero intensity at the phase singularity of the OAM beams. Also, the angular representation (plane wave expansion) of OAM beams is complex and changes drastically as the topological charges of OAM beams change. The interference of the backward scattering fields from these plane-wave rays will significantly modify the scattering feature from a simple plane-wave ray.

In this letter, motivated by the spatial phase difference of OAM beams, the scattering of electrically large standard objects at microwave frequencies is studied. To reveal the basic high-frequency scattering characteristics, we focus on two standard objects, i.e., the perfect electrical conductor (PEC) sphere and the PEC cone. The incident vortex field is generated by Hertzian dipole arrays, and the physical optics (PO) simulation of the scattered field is studied. Moreover, the characteristics of the scattered field and the RCS are analyzed. Finally, the conclusions are drawn.

## II. METHOD

In this section, a dipole array is used to generate the incident vortex field [3], [9], and the scattered field is calculated by PO approximation algorithm with the help of dyadic Green's functions [10]. The schematic for the high-frequency scattering of the PEC sphere is shown in Fig. 1. The PEC sphere is placed at the origin in the Cartesian coordinate, and the radius of the sphere is denoted as  $a$ . A uniform circular array (UCA) composed of dipoles is located on a plane parallel to the  $xoy$  plane and centered on the  $z$ -axis. The choice of the dipole orientation in Fig. 1 is motivated by the need to preserve the axial symmetry and, therefore, the OAM purity of the incident field [11], [12]. The radius of the UCA is  $r_a$ , the number of dipoles is denoted by  $N$ , and the distance between the center of the UCA and the origin is  $R_z$ . To generate OAM beams, the current density  $\mathbf{J}(\mathbf{r}_n)$  for the  $n$ th Hertzian dipole is set as

$$\mathbf{J}(\mathbf{r}_n) = \hat{\mathbf{y}} \exp(i l \phi_n) \delta(\mathbf{r} - \mathbf{r}_n) \quad (1)$$

Manuscript received April 11, 2020; revised May 5, 2020; accepted May 6, 2020. Date of publication May 11, 2020; date of current version July 7, 2020. This work was supported in part by the National Natural Science Foundation of China under Grant 61801486 and Grant 61921001 and in part by the Postdoctoral Innovative Talents Support Program of China under Grant BX20190092. (Corresponding author: Kang Liu.)

Kang Liu, Hongyan Liu, Yongqiang Cheng, and Hongqiang Wang are with the College of Electronic Science and Technology, National University of Defense Technology, Changsha 410073, China (e-mail: liukang1117@126.com; llyan1993@126.com; nudtyqcheng@gmail.com; oliverwhq@vip.tom.com).

Wei E. I. Sha is with the Key Laboratory of Micro-nano Electronic Devices and Smart Systems of Zhejiang Province, College of Information Science and Electronic Engineering, Zhejiang University, Hangzhou 310027, China (e-mail: weisha@zju.edu.cn).

Digital Object Identifier 10.1109/LAWP.2020.2993687

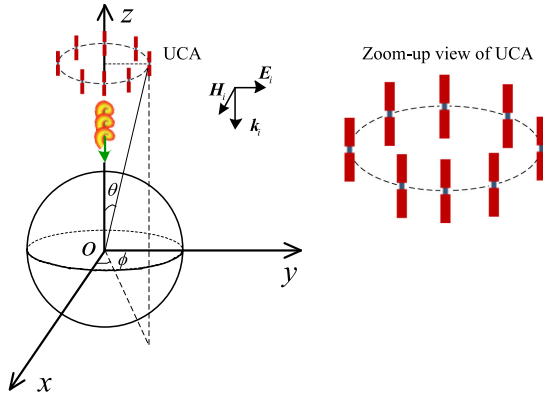


Fig. 1. Schematic for the high-frequency scattering of the PEC sphere.

where  $\mathbf{r}_n$  indicates the position of the  $n$ th dipole, and  $\mathbf{r}$  is the position vector of arbitrary point.  $\phi_n$  denotes the azimuthal angle of the  $n$ th dipole, and  $l$  signifies the topological charge of OAM beams.

According to the Helmholtz equation [13], the vector potential for the  $n$ th dipole is

$$\mathbf{A}(\mathbf{r}) = \mu \iiint \mathbf{J}(\mathbf{r}_n) g(\mathbf{r}, \mathbf{r}_n) dv_n \quad (2)$$

where  $\mu$  is the magnetic permeability and  $v_n$  indicates the integration cell of the space where the source exists.  $g(\mathbf{r}, \mathbf{r}_n)$  is the scalar Green's function, i.e.,

$$g(\mathbf{r}, \mathbf{r}_n) = \exp(ik|\mathbf{r} - \mathbf{r}_n|)/4\pi|\mathbf{r} - \mathbf{r}_n|. \quad (3)$$

The generated magnetic field for the  $n$ th dipole can be given by

$$\mathbf{H}_i^n = \frac{1}{\mu} \nabla \times \mathbf{A} = \iiint \nabla g(\mathbf{r}, \mathbf{r}_n) \times \mathbf{J}(\mathbf{r}_n) dv_n. \quad (4)$$

Considering the high-frequency scattering of electrically large objects for radar applications, the PO approximation [10] is usually applied for the calculation of the target scattering problem. The induced current density by the  $n$ th dipole at the surface of the PEC object can be approximated as

$$\mathbf{J}_s^n(\mathbf{r}') \approx \begin{cases} 2\hat{\mathbf{n}} \times \mathbf{H}_i^n|_s, & \text{illuminated regions} \\ 0, & \text{others} \end{cases} \quad (5)$$

where  $\hat{\mathbf{n}}$  is the unit vector perpendicular to the object surface and  $\mathbf{r}'$  is the position of the PEC object.

The scattered magnetic field can be calculated by the Stratton–Chu equation

$$\begin{aligned} \mathbf{H}_s^n(\mathbf{r}') &= \iint_S \mathbf{J}_s^n(\mathbf{r}') \times \nabla' g(\mathbf{r}, \mathbf{r}') dS \\ &= 2 \iint_S [\hat{\mathbf{n}} \times \mathbf{H}_i^n] \times \nabla' g(\mathbf{r}, \mathbf{r}') dS \end{aligned} \quad (6)$$

where  $S$  indicates the integration cell of the object surface illuminated by the incident field.

Based on (4) and (6), the total incident field  $\mathbf{H}_i$  and the total scattered field  $\mathbf{H}_s$  can be obtained by vector superposition of the dipole array. Then, the RCS  $\sigma$  can be calculated using the

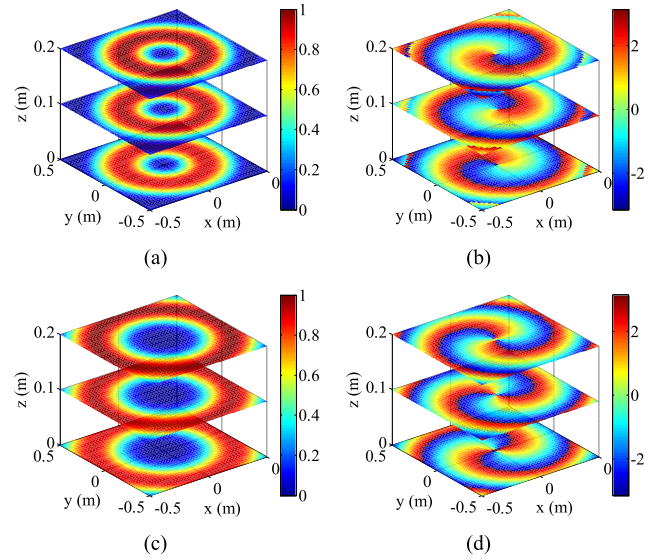


Fig. 2. Intensity and phase distributions of the incident electric field (y component). (a) Intensity  $l = 1$ . (b) Phase  $l = 1$ . (c) Intensity  $l = 2$ . (d) Phase  $l = 2$ .

TABLE I  
MAIN SIMULATION PARAMETERS

Parameter	Symbol	Value
Frequency	$f$	10 GHz
Dipole number of UCA	$N$	16
Radius of UCA	$r_a$	0.15 m
Distance between the center of UCA and the object	$R_z$	5 m

definition [10]

$$\sigma = \lim_{R_z \rightarrow \infty} 4\pi R_z^2 \frac{|\mathbf{H}_s|^2}{|\mathbf{H}_i|^2}. \quad (7)$$

### III. RESULTS AND DISCUSSION

In this part, simulations are performed to analyze the characteristics of the incident and the scattered fields. The RCSs of the PEC sphere and the PEC cone illuminated by OAM beams are estimated, respectively. The intensity and phase distributions of the incident fields are shown in Fig. 2. The main simulation parameters are listed in Table I. It can be seen that the radiation of OAM beams shows helical wavefronts in the free space, which is different from the plane wave illumination [4]. Generally, the divergence angle of the radiation pattern and the variance period of the phase are related to the topological charge.

According to the parameters listed in Table I, the phase profiles of the scattered field are shown in Fig. 3. In contrast to the illumination of the plane wave, results indicate that the scattered field still follows a helical structure corresponding to the topological charge of the incident field. This result can be understood by the angular momentum conservation [14] by collimating the OAM beam axial and symmetric axial of the sphere. Furthermore, the OAM spectra [15] of the scattered field are shown in Fig. 4. The scattered field is sampled along with a circle and fast Fourier transform is performed on the

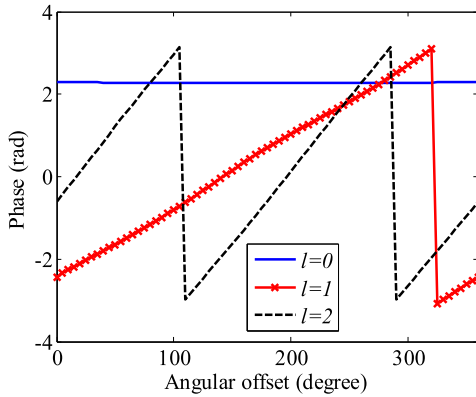


Fig. 3. Phase profiles of the scattered field from a PEC sphere with the radius of 0.2 m.

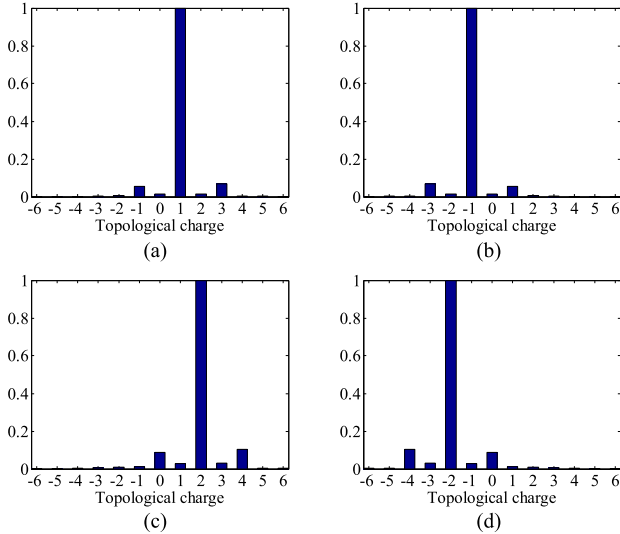


Fig. 4. OAM spectra of the scattered field. (a)  $l = 1$ . (b)  $l = -1$ . (c)  $l = 2$ . (d)  $l = -2$ .

sampled data. Since the scattered field can hardly be written in an analytical expression, the OAM spectra can generally be obtained by numerical methods. For the PEC sphere, the scattered field of the OAM's illumination is also a vortex field, and the topological charge is almost the same as that of the incident field. It is also noted that a weak mixing of the OAM spectra occurs, which is mainly caused by the calculation error of the scattered field.

For plane-wave illumination, the RCS for the PEC sphere can be calculated by the Mie theory [16], i.e.,

$$\sigma = \frac{\lambda^2}{\pi} \left| \sum_{n=1}^{\infty} (-1)^n (n + 0.5) (b_n - a_n) \right|^2 \quad (8)$$

where

$$\begin{aligned} a_n &= -\frac{\hat{J}'_n(ka)}{\hat{H}_n^{(1)'}(ka)} \omega_n, \quad b_n = -\frac{\hat{J}_n(ka)}{\hat{H}_n^{(1)}(ka)} \omega_n \\ \omega_n &= \frac{(-i)^{-n} (2n + 1)}{n(n + 1)}. \end{aligned} \quad (9)$$

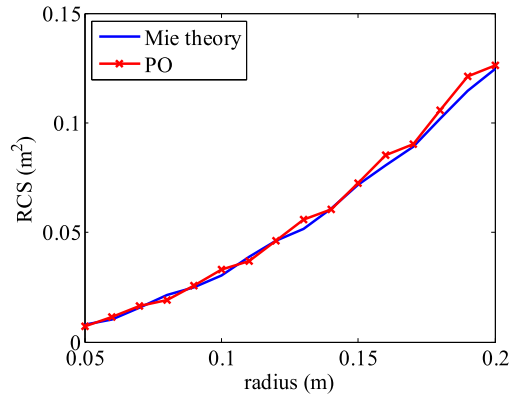


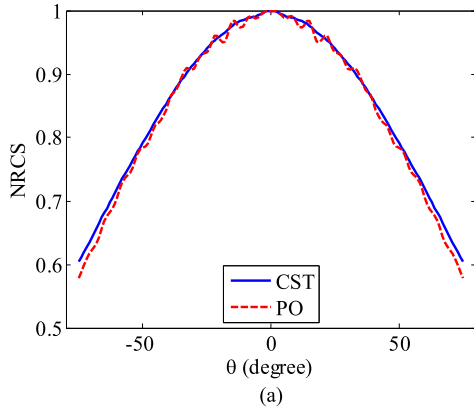
Fig. 5. RCS as a function of the sphere radius for  $l = 0$ .

To validate the accuracy of the proposed method, the RCSs of the PEC sphere from the backward scattering are provided, as shown in Fig. 5. As for the illumination of the plane wave, the NRCS is equal to the well-known value of  $\pi a^2$ . It can be seen from Fig. 5 that two RCS curves fit well to each other, which verifies the accuracy of the proposed method.

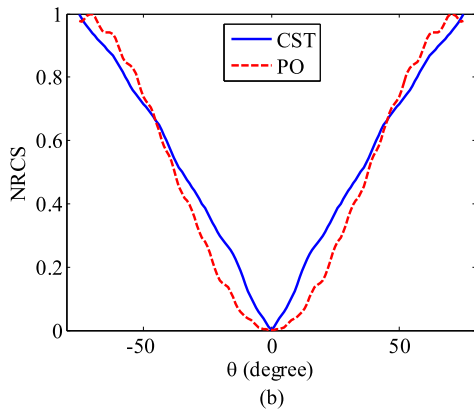
The normalized radar cross section (NRCS) from different scattering angles is shown in Fig. 6. For  $l = 0$ , the maximum value of the NRCS is located at the position  $\theta = 0^\circ$ , which indicates that the backward scattering for plane wave illumination is stronger than other directions. It is clear that the calculation results of the proposed method fit well with the full-wave simulation results by CST. The differences between the two curves are mainly caused by the nonideal effect during the generation of OAM beams. In contrast to the plane wave, the minimum value for OAM beams occurs in the backscattering direction, which is mainly caused by the phase singularity of OAM beams, as illustrated in Fig. 6.

The scattering of OAM beams by PEC cone is also studied, and the schematic for cone scattering is shown in Fig. 7. The bottom radius of the cone is set as 0.1 m, and the height is 0.2 m. The phase profiles of the scattered electric field ( $y$  component) for different OAM modes are depicted in Fig. 8, and the OAM spectra are shown in Fig. 9. Similar to the sphere scattering, the scattered field for PEC cone is also a vortex field. Thus, for the axial symmetric object, it can be concluded that the scattered field will maintain the OAM characteristics. However, for a non-symmetric object, the significant OAM spectra mixing will occur.

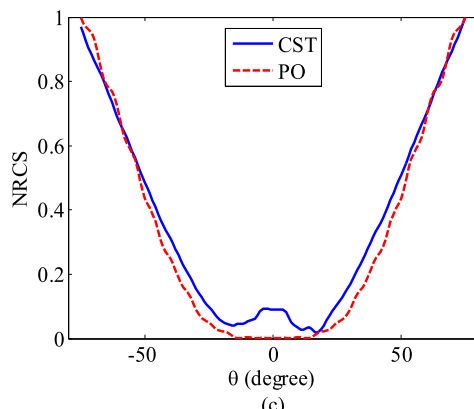
The NRCS for the PEC cone as a function of the scattering angle is shown in Fig. 10. The maximum value occurs at the angle of  $\theta = 0^\circ$  for  $l = 0$ . Similarly, the minimum value occurs for OAM beams' illumination. For OAM beams, the maximum direction is dependent on the topological charge, i.e., high-order topological charge leads to large scattering angle. Compared to the PEC sphere, the backward RCS of PEC cone shows many ripples. The induced current highly depends on the normal vector of the surface, as shown in (5). For the cross section at the  $yoz$  or  $xoz$  plane, the normal vector of the cone is constant but that of sphere is gradually changed. Thus, the constructive interference of the induced current at the surface of the PEC cone occurs at specific angles due to the identical amplitude and direction of the induced current.



(a)



(b)



(c)

Fig. 6. NRCS as a function of the scattering angle. (a)  $l = 0$ . (b)  $l = 1$ . (c)  $l = 2$ .

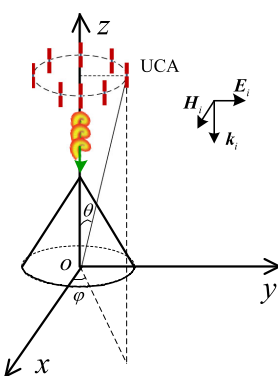


Fig. 7. Schematic for the scattering of PEC cone.

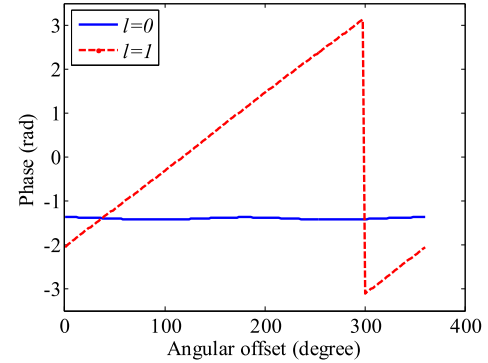


Fig. 8. Phase profiles for cone scattering field.

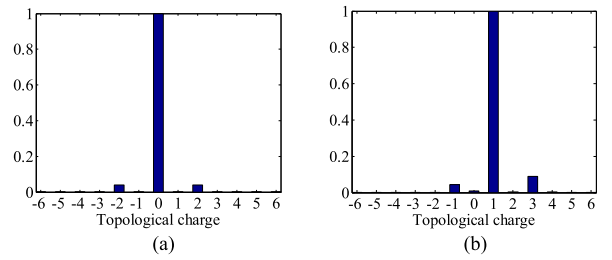


Fig. 9. OAM spectra of the cone scattering field. (a)  $l = 0$ . (b)  $l = 1$ .

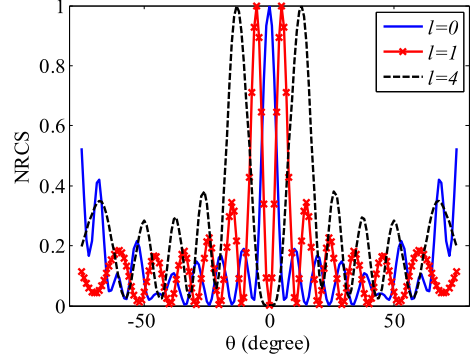


Fig. 10. NRCS for PEC cone as a function of the scattering angle.

#### IV. CONCLUSION

In this letter, the backward scattering of OAM beams by two standard objects at microwave frequencies has been studied. The incident vortex field was generated by a dipole array, and the scattered field was calculated by the PO algorithm. Theoretical and simulation results indicated that the scattered field of OAM beam by an axial symmetric object is still a vortex field when the phase singularity point of OAM beams is aligned to the symmetric axis. And the topological charge of the scattered field is the same as that of the incident field. For the PEC sphere and PEC cone, the RCS characteristics are different from the plane wave illumination, and the direction angle of the maximum NRCS value changes significantly with the topological charge. The results in this letter can benefit the design of the OAM-based radar system and radar target detection. In future work, the scattering of complex structured objects by OAM beams will be studied.

## REFERENCES

- [1] D. Lee, *et al.*, “An experimental demonstration of 28 GHz band wireless OAM-MIMO multiplexing,” in *Proc. IEEE 87th Veh. Technol. Conf.*, 2018, doi: [10.1109/VTCSpring.2018.8417790](https://doi.org/10.1109/VTCSpring.2018.8417790).
- [2] M. P. J. Lavery, F. C. Speirits, S. M. Barnett, and M. J. Padgett, “Detection of a spinning object using light’s orbital angular momentum,” *Science*, vol. 341, no. 6145 pp. 537–540, Aug. 2013.
- [3] K. Liu, Y. Cheng, Z. Yang, H. Wang, Y. Qin, and X. Li, “Orbital-angular-momentum-based electromagnetic vortex imaging,” *IEEE Antennas Wireless Propag. Lett.*, vol. 14, pp. 711–714, 2015.
- [4] K. Liu, Y. Q. Cheng, X. Li, and Y. Gao, “Microwave-sensing technology using orbital angular momentum: Overview of its advantages,” *IEEE Veh. Technol. Mag.*, vol. 14, no. 2, pp. 112–118, Jun. 2019.
- [5] F. G. Mitri, “Arbitrary scattering of an electromagnetic zero-order Bessel beam by a dielectric sphere,” *Opt. Lett.*, vol. 36, no. 5, pp. 766–768, 2011.
- [6] W. Sun, Y. Hu, and C. Weimer, “FDTD modeling of OAM beam’s interaction with dielectric particle,” in *Proc. Prog. Electromagn. Res. Symp.*, Shanghai, China, Aug. 2016, p. 3295, doi: [10.1109/PIERS.2016.7735288](https://doi.org/10.1109/PIERS.2016.7735288).
- [7] B. Tang, B. Jian, and X. Sheng, “Orbital-angular-momentum-carrying wave scattering by the chaff clouds,” *IET Radar, Sonar Navig.*, vol. 12, no. 6, pp. 649–653, 2015.
- [8] X. Bu, Z. Zhang, X. Liang, Z. Zeng, L. Chen, and H. Tang, “Scattering characteristics of vortex electromagnetic waves for typical targets,” in *Proc. Asian-Pac. Microw. Conf.*, 2018, pp. 648–650.
- [9] B. Thidé *et al.*, “Utilization of photon orbital angular momentum in the low-frequency radio domain,” *Phys. Rev. Lett.*, vol. 99, no. 8, 2007, Art. no. 087701.
- [10] E. F. Knott, J. F. Shaeffer, and M. T. Tuley, *Radar Cross Section*, 2nd ed. Raleigh, NC, USA: SciTech, 2004.
- [11] A. Cagliero, “Symmetry breaking in UCA-based vortex waves,” *J. Phys. Commun.*, vol. 2, no. 9, 2018, Art. no. 095012.
- [12] K. Liu *et al.*, “Generation of OAM beams using phased array in the microwave band,” *IEEE Trans. Antennas Propag.*, vol. 64, no. 9, pp. 3850–3857, Sep. 2016.
- [13] C. A. Balanis, *Advanced Engineering Electromagnetic*, New York, NY, USA: Wiley, 1989.
- [14] X. Y. Xiong, A. Al-Jarro, L. J. Jiang, N. C. Panoiu, and W. E. I. Sha, “Mixing of spin and orbital angular momenta via second-harmonic generation in plasmonic and dielectric chiral nanostructures,” *Phys. Rev. B*, vol. 95, 2017, Art. no. 165432.
- [15] F. Tamburini, E. Mari, B. Thidé, C. Barbieri, and F. Romanato, “Experimental verification of photon angular momentum and vorticity with radio techniques,” *Appl. Phys. Lett.*, vol. 99, 2011, Art. no. 204102.
- [16] J. J. Bowman, T. B. A. Senior, and P. L. E. Uslenghi, *Electromagnetic and Acoustic Scattering by Simple Shapes*. Amsterdam, The Netherlands: North-Holland, 1969.